Chemistry–A European Journal

Research Article
doi.org/10.1002/chem.202302979

Chemistry Europe
European Chemical Societies Publishing

www.chemeurj.org

Hot Paper

Development of Novel Redox-Active Organic Materials Based on Benzimidazole, Benzoxazole, and Benzothiazole: A Combined Theoretical and Experimental Screening Approach

Xhesilda Fataj,[a, b] Andreas J. Achazi,[c, d] Philip Rohland,[a, b] Erik Schröter,[a, b] Simon Muench,[a, b] René Burges,[a, b] K. Linus H. Pohl,[c, d] Doreen Mollenhauer,[c, d] Martin D. Hager,[a, b] and Ulrich S. Schubert*[a, b]

Sustainability is one of the hot topics of today's research, in particular when it comes to energy-storage systems such as batteries. Redox-active molecules implemented in organic batteries represent a promising alternative to lithium-ion batteries, which partially rely on non-sustainable heavy metal salts. As an alternative, we propose benzothiazole, -oxazole and -imidazole derivatives as redox-active moieties for polymers in organic (radical) batteries. The target molecules were identified by a combination of theoretical and experimental approaches for the investigation of new organic active materials. Herein, we present the synthesis, electrochemical characterization and theoretical investigation of the proposed molecules, which can later be introduced into a polymer backbone and used in organic polymer batteries.

Introduction

Renewable energy storage is one of the most urgent challenges of the 21st century. For environmental, economic, and political reasons, consuming less energy from fossil sources and focusing on more sustainable, clean energy sources is required. To match the requirements of sustainable energy production, ideally, energy storage must also take place under environmentally friendly conditions.[1–2] For this, toxic and non-sustainable heavy metals, such as copper, cobalt or manganese, must be excluded from energy storage devices.[3] Along goes, the increasing digitalization of our everyday life results in increasing energy demand and a high requirement for small-scale energy storage.[4] Currently, the need for small-scale energy storage is mostly met by lithium-ion batteries. However, they contain manganese or cobalt-bearing materials, additionally, there are concerns about the safety, reliability, and performance degradation of the Li-ion batteries. To overcome this issue, alternative eco-friendly and cost-effective battery technologies are widely investigated. As low-toxic and abundant materials, organic redox-active materials implemented in organic polymer batteries have gained extensive interest over the last years.[5–7]

Generally, organic polymer batteries are made from organic materials, that may be obtained from renewable sources via synthetic routes in the near future. No transition metals are needed and, instead, redox-active organic materials are used. Recently, intensive research has been performed on organic polymers with different redox-active moieties as the active compounds in composite electrodes. Here, polymers combine the required reversible redox activity with the necessary insolubility of the active material in the battery electrolyte.[8–11] One of the established organic anode materials relies on 4,4'-bipyridine units (=viologen) within the main or side chain of the polymer. These materials have been investigated by several research groups and have been proven to be compatible with aqueous electrolytes.[12–15]

Viologens have been used as anode material mainly in polymer-based and redox-flow batteries. However, when the material is implemented in solid organic electrodes, only a limited chain length of the polymers has been presented, which can result in undesired active material dissolution in the battery electrolyte. This can lead to shuttling processes and a pronounced self-discharge of the battery cell.[16] Furthermore,

[a] X. Fataj, Dr. P. Rohland, E. Schröter, Dr. S. Muench, R. Burges, Dr. M. D. Hager, Prof. U. S. Schubert
Laboratory of Organic and Macromolecular Chemistry (IOMC)
Friedrich Schiller University Jena
Humboldtstraße 10, 07743 Jena (Germany)
E-mail: ulrich.schubert@uni-jena.de

[b] X. Fataj, Dr. P. Rohland, E. Schröter, Dr. S. Muench, R. Burges, Dr. M. D. Hager, Prof. U. S. Schubert
Center for Energy and Environmental Chemistry Jena (CEEC Jena)
Friedrich Schiller University Jena
Philosophenweg 7a, 07743 Jena (Germany)

[c] Dr. A. J. Achazi, K. L. H. Pohl, Prof. D. Mollenhauer
Institute of Physical Chemistry
Justus-Liebig University Giessen
Heinrich-Buff-Ring 17, 35392 Gießen (Germany)

[d] Dr. A. J. Achazi, K. L. H. Pohl, Prof. D. Mollenhauer
Center for Materials Research
Justus-Liebig University Giessen
Heinrich-Buff-Ring 16, 35392 Giessen (Germany)

Supporting information for this article is available on the WWW under https://doi.org/10.1002/chem.202302979

© 2023 The Authors. Chemistry - A European Journal published by Wiley-VCH GmbH. This is an open access article under the terms of the Creative Commons Attribution Non-Commercial License, which permits use, distribution and reproduction in any medium, provided the original work is properly cited and is not used for commercial purposes.

© 2023 The Authors. Chemistry - A European Journal published by Wiley-VCH GmbH

the stability of solid-state electrodes containing viologen as the active material (Scheme 1), is an issue of on-going investigation.[17] Additionally, small molecular viologen compounds exhibit high toxicity.[14]

Much research has been performed to improve their properties by modification of the structure leading to difficult synthetic routes and stability problems.[19–20] This highlights the need for alternative compounds that are compatible with established cathode materials and can compete with the redox chemistry of viologen. In particular, pyridine-based systems have been successfully studied as redox-active materials, for example, benzoylpyridinium salts, which were also identified in a combined experimental and theoretical approach.[21–23]

Here, we present new anode materials, pyridinium-substituted molecules inspired by viologen, namely 4-(benzo[*d*]**thiazol**-2-yl)-1-methylpyridin-1-ium chloride, 4-(benzo[*d*]**oxazol**-2-yl)-1-methylpyridin-1-ium chloride, and 4-(1*H*-benzo[*d*]**imidazol**-2-yl)-1-methylpyridin-1-ium chloride. The structures were derived from viologen by substituting one of the pyridinium rings with -thiazole, -oxazole and -imidazole. Interestingly, despite their promising electrochemical properties, these materials have not yet been studied for polymer-based batteries. For example, benzimidazole lithium salts have been studied as electrolytes for lithium-ion batteries or as special derivatives as n-type semiconductors.[24,25] These heteroaromatic moieties are mostly used as building blocks for the synthesis of more complex molecules for biological applications, such as anti-inflammatory, anticancer, antibacterial, and antifungal applications.[26]

In the search for new materials, computational methods, and molecular modeling contribute to the understanding, screening, and design of organic active materials.[27–29] For computational high-throughput screening, it is advantageous if the basic molecule to be screened and the underlying redox reaction have already been studied experimentally. This helps to validate the theoretical methodological approach and to estimate the stability of the molecule class or to identify side reactions that need to be considered. In addition, possible interactions with compounds in solution or dimerization effects can be worked out in a joint experimental and theoretical effort. In this context, we present here the synthesis of the basic molecules **1**–**9** (Figure 1). These structures were subjected to in-detail analysis via cyclic voltammetry (CV) in a standardized three-electrode setup. CV was mainly chosen as a characterization method because it is often one of the first experiments performed in an electrochemical study of a new redox-active compound. Its good sensitivity, variable time scale, and the obtained information over a wide potential range regarding reducible or oxidizable species make it the most versatile

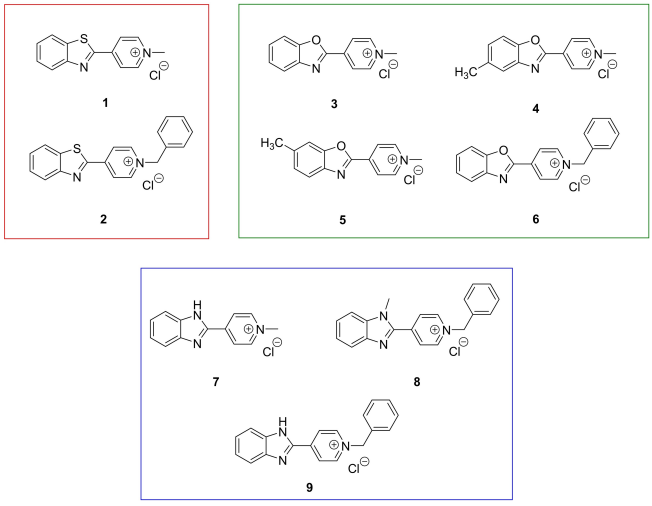

Figure 1. Schematic representation of the synthesized molecules. Thiazoles: **1**: 4-(benzo[*d*]thiazol-2-yl)-1-methylpyridin-1-ium chloride, **2**: 4-(benzo[*d*]thiazol-2-yl)-1-benzylpyridin-1-ium chloride; oxazoles: **3**: 4-(benzo[*d*]oxazol-2-yl)-1-methylpyridin-1-ium chloride, **4**: 1-methyl-4-(5-methylbenzo[*d*]oxazol-2-yl)pyridin-1-ium chloride, **5**: 1-methyl-4-(6-methylbenzo[*d*]oxazol-2-yl)pyridin-1-ium chloride. **6**: 4-(benzo[*d*]oxazol-2-yl)-1-benzylpyridin-1-ium chloride; imidazoles: **7**: 4-(1*H*-benzo[*d*]imidazol-2-yl)-1-methylpyridin-1-ium chloride, **8**: 1-benzyl-4-(1-methyl-1*H*-benzo[*d*]imidazol-2-yl)pyridin-1-ium chloride, **9**: 4-(1*H*-benzo[*d*]imidazol-2-yl)-1-benzylpyridin-1-ium chloride.

electroanalytical technique.[30] By this means, we evaluated the feasibility of a new functional group for an introduction into or onto a polymeric backbone. The experimental results are compared to the calculated results of the redox potentials at DFT-D3 level of theory. The aim is to gain a deeper understanding of the redox reactions. The understanding of the redox reactions and the experimental data as a reference point will be used to start computational high-throughput screening of molecules with the basic structures shown in (Figure 1) in future investigations.[31]

Results and Discussion

Synthesis

Scheme 2 summarizes the synthetic route for the targeted compounds. The synthesis of benzothiazole and benzimidazole was performed by the condensation of 4-pyridinecarboxaldehyde with 2-aminothiophenol and *o*-phenylenediamine. The benzoxazole derivatives were synthetically obtained in a straightforward condensation reaction in poly(phosphoric acid)

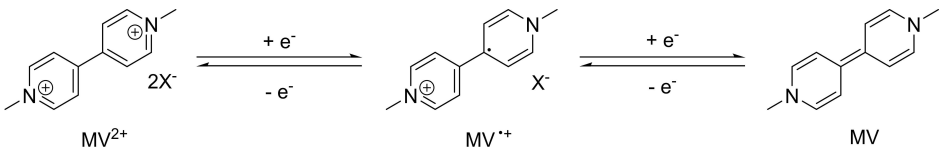

Scheme 1. Schematic representation of the methyl viologen structure and its redox chemistry.[18]

© 2023 The Authors. Chemistry - A European Journal published by Wiley-VCH GmbH

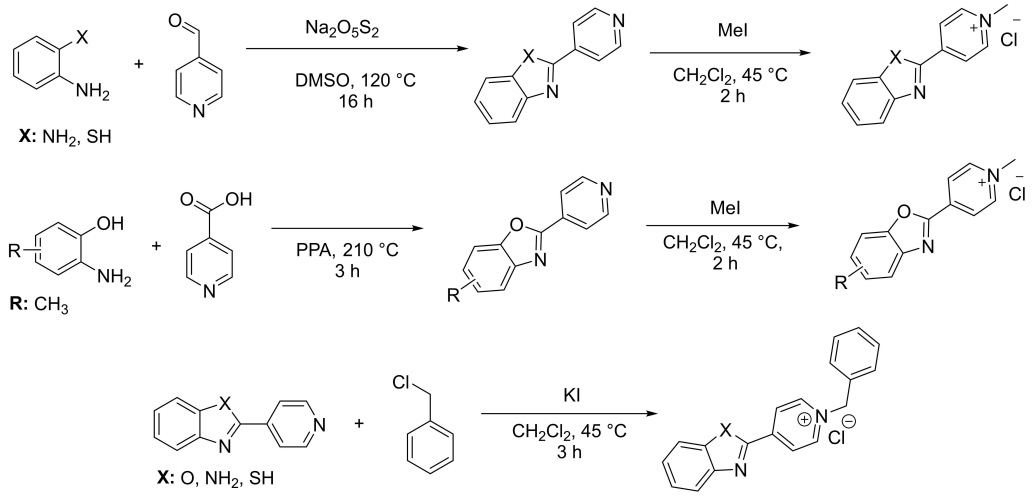

Scheme 2. Schematic representation of the synthesis of the core molecules and of charge introduction by methylation and benzylation.

(PPA) from the 2-aminophenol precursors and isonicotinic acid.[32–33]

This reaction was performed for 2-phenylbenzo[*d*]oxazole, 5-methyl-2-phenylbenzo[*d*]oxazole, and 6-methyl-2-phenylbenzo[*d*]oxazole, which yielded the products in high yields of 83, 89, and 91 %, respectively. In order to yield the corresponding cationic pyridinium compounds, the compounds were N-methylated at the pyridine nitrogen atom. As an alternative for methylation, N-benzylation was performed to obtain a model compound for a possible monomer synthesis in the future, comparable to the polyviologens with polystyrenic backbone.[12,13]

To confirm the chemical structure and the purity of the material, characterization methods such as ^{1}H and ^{13}C NMR spectroscopy, elemental analysis, liquid chromatography, and HRMS spectrometry were performed. A minimum of three different characterization methods per molecule was executed (see the Supporting Information for details).

Table 1. Reduction and oxidation potentials calculated at BP86-D3(BJ)/def2-TZVP (DCOSMO-RS-outercharge: CH_3CN) level of theory. A model of a single molecule being oxidized or reduced is used. The value in square brackets is the potential when the dimer formation (Scheme 4b) is included.

		$E_{1/2}$ reduction in V		$E_{1/2}$ oxidation in V	
X	Rest	Exp.	Calcd	Exp	Calcd
1. S	Me	−1.80	−1.80	−1.11	−1.10
2. S	Bn	−1.75	−1.77	−1.07	−1.07
3. O	Me	−1.85	−1.84	−1.10	−1.10
4. O–CH_3	Me	−1.87	−1.86	−1.12	−1.11
5. O–CH_3	Me	−1.87	−1.88	−1.12	−1.13
6. O	Bn	−1.81	−1.82	−1.05	−1.06
7. N–H	Me	−1.95	−2.07 [−1.96]	−1.30	−1.31
8. N–CH_3	Bn	−2.03	−2.02	−1.29	−1.30
9. N–H	Bn	−2.07	−2.03	−1.27	−1.29

Electrochemical characterization

For the investigation of the electrochemical properties, CV measurements were performed in solution using a three-electrode setup. For this, a $Ag/AgNO_3$ (0.01 M) reference electrode, a platinum wire as a counter electrode and a glassy carbon electrode as working electrode were used. The materials were measured in 0.1 M $TBAPF_6$ in acetonitrile (CH_3CN). CH_3CN was the solvent of choice since was one of the solvents to interact best with all nine molecules. Furthermore, $TBAPF_6$ is a non-coordinating electrolyte ion and CH_3CN is aprotic, which is beneficial for the computational investigation. The results obtained from this investigation were compared to the theoretical potential values (Table 1).

The benzothiazole derivatives **1** and **2** exhibit a defined peak shape in the CVs (Figure 2). In particular, the methylated derivative leads to two narrow redox signals corresponding to half-wave potentials of −1.11 and −1.80 V vs. $Ag/AgNO_3$ (Table 1) for the first and second reduction/oxidation peaks at different scanning rates. On the other hand, the benzylated derivative exhibits a reversible behavior at lower scanning rates (50, 100, 200 mV s^{-1}) corresponding to half-wave potentials of −1.07 and −1.75 V for the first and second reduction/oxidation peaks but a non-reversible behavior at higher scanning speeds (500, 1000, 2000 mV s^{-1}). The corresponding theoretical and experimental half-wave potentials for the two reversible peaks are given in Table 1. The first and second reduction/oxidation peaks agree well with the theoretical values.

Figure 3 shows the cyclic voltammograms of the benzoxazole derivatives. The data reveals for **3**–**6** a reversible peak shape with half-wave potentials of −1.05 to −1.12 V and −1.81 to −1.87 V (Table 1) for the first and second reduction/oxidation peak at different scanning rates. In general, **4** and **5** exhibit the same half-wave potentials (oxidation $E_{1/2} = -1.12$ V and reduction $E_{1/2} = -1.87$ V) at different scanning rates. For the oxazole molecules **3**–**6** the calculated reduction and oxidation poten-

© 2023 The Authors. Chemistry - A European Journal published by Wiley-VCH GmbH

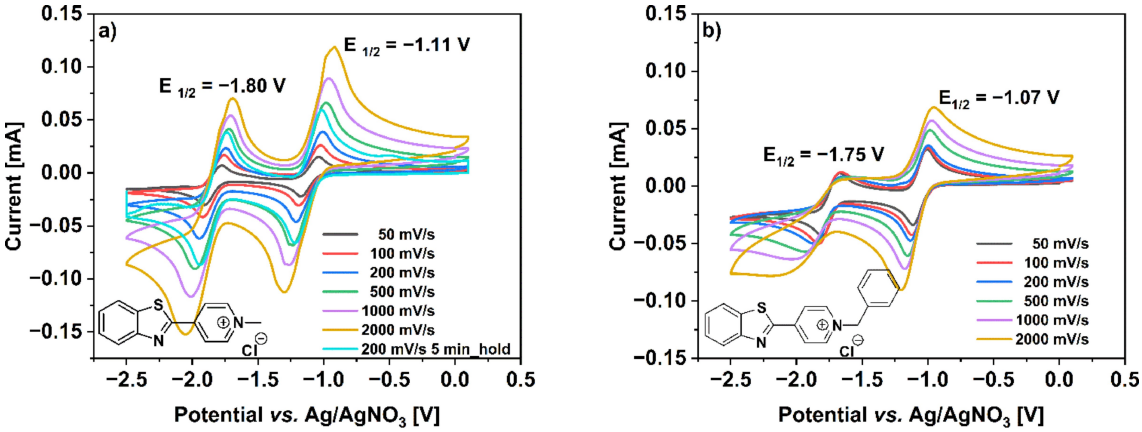

Figure 2. Cyclic voltammetry measurements of benzothiazole derivates a) **1** and b) **2** at different scanning speeds using 0.1 M $TBAPF_6$ in CH_3CN as supporting electrolyte. Associated half wave potentials for (a) are given in Table 1.

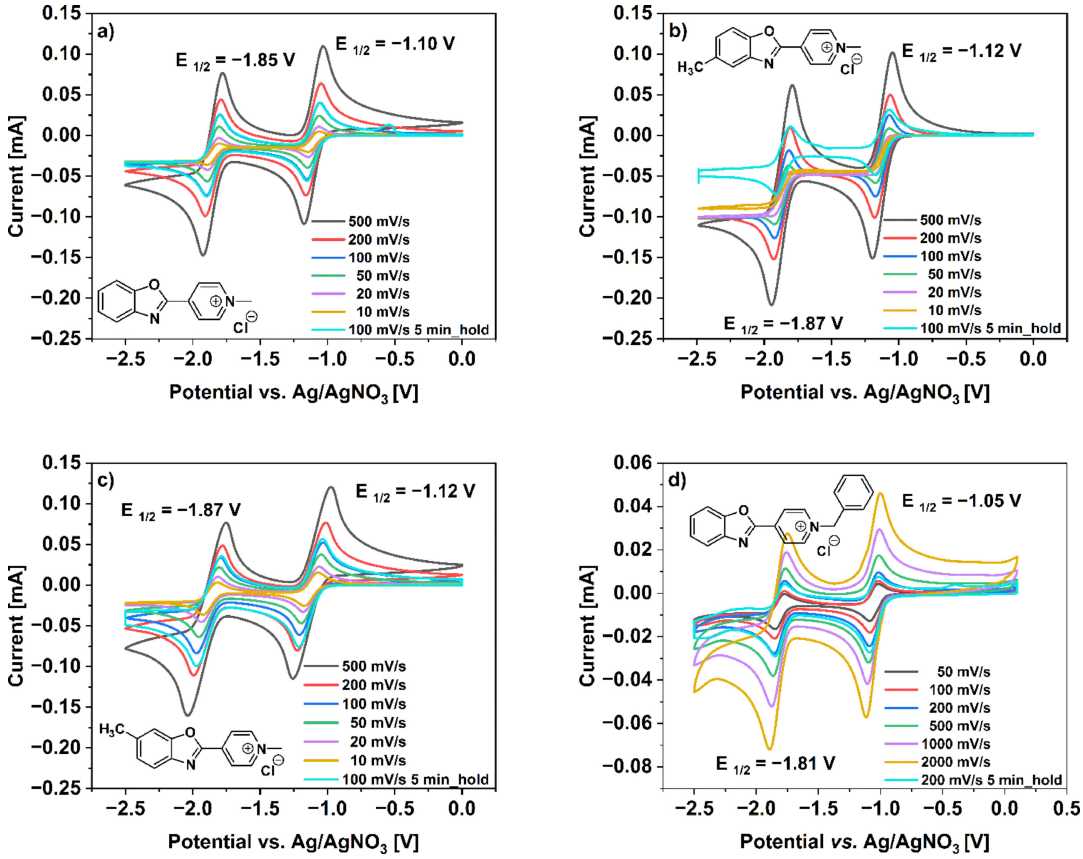

Figure 3. Cyclic voltammetry measurements of benzoxazoles a) **3**, b) **4** c) **5** and d) **6** at different scanning speeds using 0.1 M $TBAPF_6$ in CH_3CN as supporting electrolyte. Associated half-wave potentials are given in Table 1.

tials (Table 1) also agree very well with the experimental values. The calculated values capture the decrease of the reduction and oxidation potentials from **3** to **4** and **5** as well as the increase of these potentials from **3** to **6** very well, despite the fact that only small changes in potential are involved.

Figure 4 shows the CVs of the synthesized imidazole derivates **7**–**9**. According to the voltammograms, the molecules do not exhibit reversible redox reactions. From the CVs it can be concluded that no defined oxidation or reduction peaks are obtained. To explain the reason behind this irreversible behavior, several theoretical investigations were performed.

Computational investigation

To gain a deeper understanding of the redox reactions, we performed theoretical calculations at the DFT level of theory. The resulting half-wave potentials from the theoretical calcu-

© 2023 The Authors. Chemistry - A European Journal published by Wiley-VCH GmbH

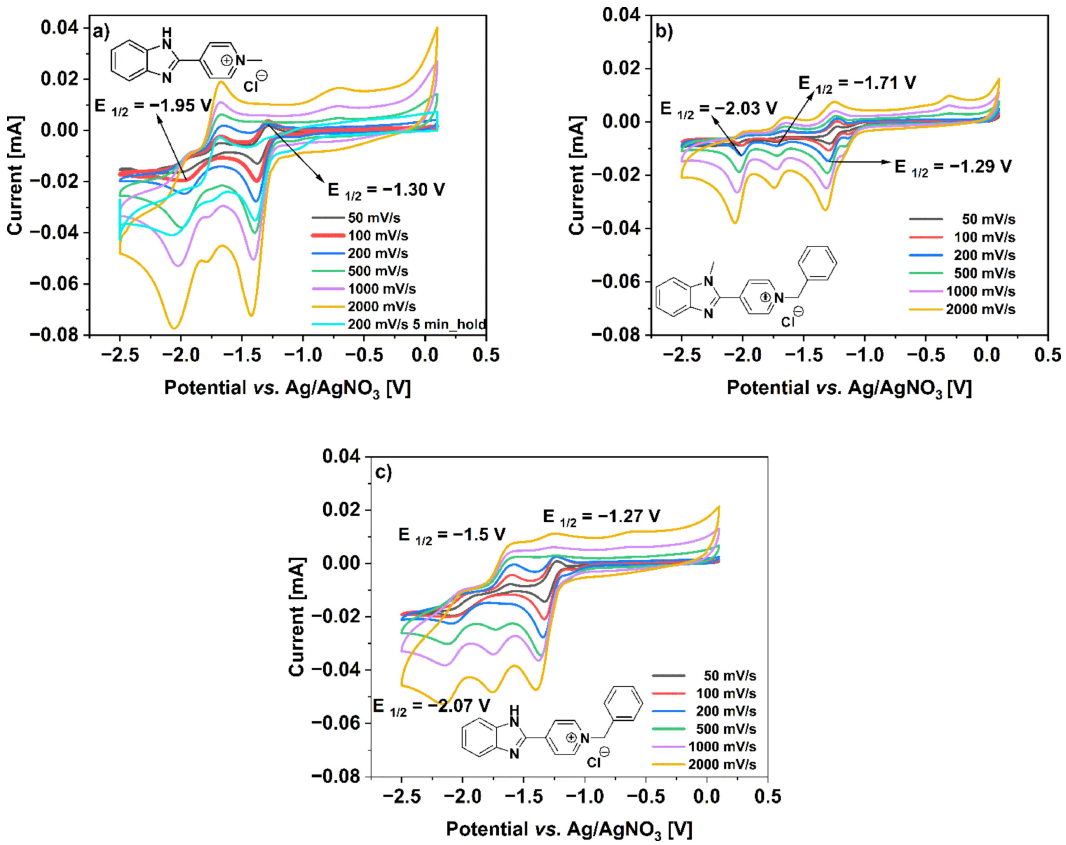

Figure 4. Cyclic voltammetry measurements of benzimidazoles derivatives a) **7**, b) **8** and c) **9** tested at different scanning speeds using 0.1 M $TBAPF_6$ in CH_3CN as supporting electrolyte. Associated half-wave potentials are given in Table 1.

lations and experiments are presented in Table 1. The expected electrochemical reactions for the three groups of molecules investigated, -thiazole, -oxazole, and imidazole, is shown in Scheme 3. The first redox reaction, from the cation to the neutral species, corresponds to the first peak of reduction or oxidation in the experimental CVs. As the neutral species is oxidized to the cation, it is referred to as $E_{1/2}$ oxidation in Table 1. The second redox reaction corresponds to the second reduction/oxidation peak observed in the experimental CVs. In Table 1, $E_{1/2}$ reduction refers to the reduction of a neutral species to the corresponding anion. The theoretically calculated potentials are determined from the calculated Gibbs energies of these expected reaction mechanism. The value in square brackets (Table 1) is the potential when dimer formation is included (Scheme 4b).

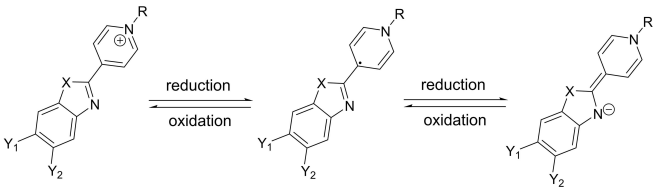

Scheme 3. Schematic representations of the investigated redox reactions of 2-(4-R-phenyl)-6-Y-benzo[*d*]-X-zole with X=O, S, NH, NMe; $Y_{1,2}$=H, Me; R=Me, Bn.

We used the experimental oxidation and reduction potentials of molecules **1**, **3**, **6**, and **7** (**7** only for the oxidation potential) for the evaluation of the DFT approach and introduced shift values for the calculated oxidation and reduction potentials (see Appendix and ref. [31]) The determined shift values change the calculated redox potentials by a fixed value that minimizes the difference between the trend lines of the experimental and the calculated redox potentials. This allows an immediate assessment of the consistency between the calculated and experimental trends. As a result, the oxidation potentials differ on average by only 7 mV and the reduction potentials on average by 8 mV from the experimental values (Table 1). For molecules **2**, **4**, **5**, **8** and **9** the average deviation of the oxidation and reduction potentials from the experimental values is 12 and 18 mV, respectively. Thus, the DFT approach is able to describe the trend of the experimental redox potentials for the different molecules. In addition, it provides accurate results by applying the determined shift value that is based on four representative molecules. The agreement between experimental and computational results is particularly high for the -thiazoles and -oxazoles that show reversible redox properties (Figures 2 and 3).

The second reduction/oxidation peak, $E_{1/2}$ reduction in Table 1 of **7**, shows a larger deviation (0.12 V) from the calculated redox potential (Scheme 4a) compared to the other molecules. Therefore, we investigated the interaction between

© 2023 The Authors. Chemistry - A European Journal published by Wiley-VCH GmbH

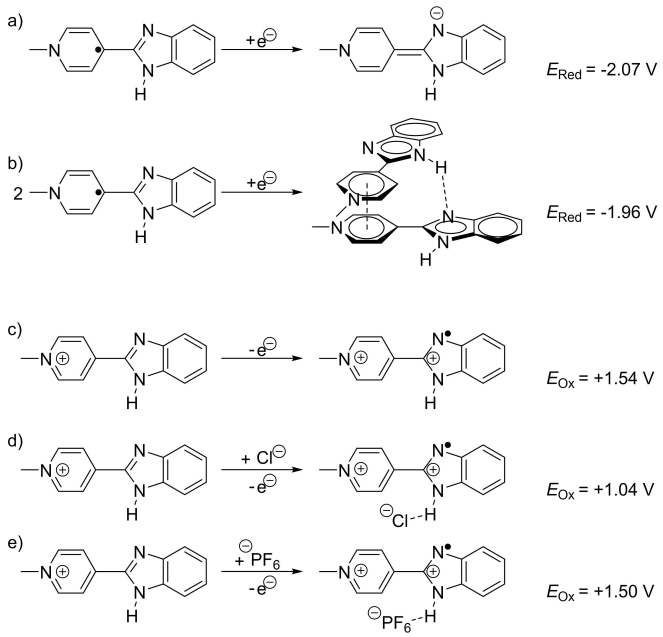

Scheme 4. Schematic representation of possible model reactions for the reduction [(a), (b)], and second oxidation [(c)–(e)] used in the calculations for **7**.

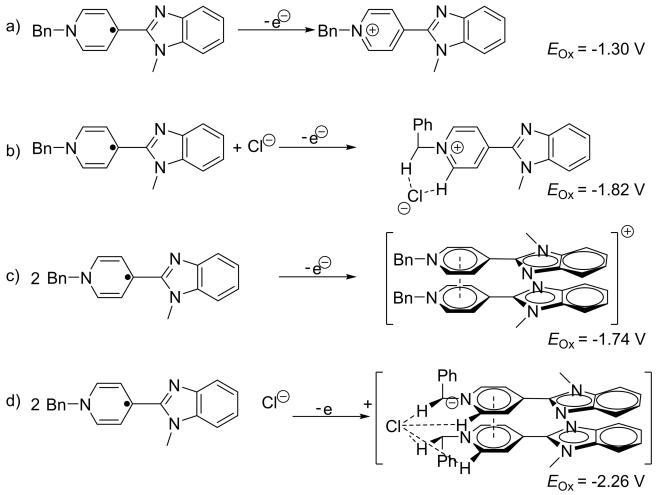

Scheme 5. Schematic representation of the investigated oxidation reaction calculated for the 1-methyl benzimidazole derivative (with X=NMe, Y=H, R=Bn).

7 and the chloride ion and the dimerization of **7**, and their influence on the second reduction/oxidation peak. Taking into account dimer formation through hydrogen bonding (Scheme 4b), we observed that the calculated second reduction/oxidation potential of **7** is in good agreement with the experimental value (deviation of 0.01 V). A possible reason that dimerization only occurs for **7** could be that it is the only protic molecule of the nine tested. The ability to form hydrogen bonds seems to be the only distinguishing factor between **7** and the other molecules.

Interestingly, there is an additional peak in the CV of **7** at +0.92 V (Figure S8 in the Supporting Information). This probably represents an oxidation of the cationic species of **7**. However, the experimental value is much lower than what was predicted by the calculation (Scheme 4c). Taking into the chloride counter ions in the calculations leads to a decrease in the oxidation potential (Scheme 4d). This is due to hydrogen bonding between the chloride anion and the NH group. In contrast, the presence of the non-coordinating ion PF_6^- show hardly any effect on the oxidation potential. If the interaction between the dication of **7** and the chloride counterion is considered, the deviation between the calculated and experimental redox potentials is much smaller but still 0.12 V. It is possible that the absence of counter ions during the method validation led to the larger deviation observed in this case.[31]

For molecule **8**, the first (−1.29 V) and third (−2.03 V) reduction/oxidation peaks are in agreement with the calculated $E_{1/2}$ oxidation and $E_{1/2}$ reduction potentials (Table 1), respectively. Nonetheless, there appears a peak at −1.71 V in between. We have considered three cases to comprehend its origin as a possible influence on the oxidation potential that could result in this peak (Scheme 5). First, the neutral molecule is oxidized to a cation that forms a contact ion pair with a chloride counter ion from the solution (Scheme 5b). With a calculated oxidation potential of E_{Ox} = −1.82 V, this model reaction deviates by −0.11 V from the experimental value. Second, two single molecules of **8** are oxidized to a cationic dimer (Scheme 5c). Here the oxidation potential (E_{Ox} = −1.74 V) differs from the experimental oxidation potential by only +0.03 V. Third, it is again assumed that a cationic dimer is formed. This time it forms a contact ion pair with a chloride counterion during oxidation (Scheme 5d). The oxidation potential (E_{Ox} = −2.26 V) differs by −0.55 V from the experimental value. Thus, the calculation suggests that the peak at −1.71 V in the CV of **8** is most likely caused by the formation of van der Waals bound dimers (Scheme 5c). The formation of contact ion pairs (Scheme 5b) exhibits a slightly larger deviation, but could also be a possible explanation since we also found a larger deviation of the complex with the chloride counter ion of **7** compared to the experimental value (Scheme 4d). One reason for the dimer or ion pair formation of **8** might be the more localized positive charge. The heteroatom X in **8** is the bulky-NMe-group. Because of this, the pyridyl and benzimidazole groups are out of plane and their π-systems overlap less. Accordingly, the benzimidazole group stabilizes the positively charged pyridyl group of the oxidized **8** less, and the oxidized **8** forms dimers with neutral **8** molecules for stabilization. The steric repulsion caused by the -NMe-group also reduces the rotational barrier of the benzimidazole derivatives as shown in Figure S7.

Structure-property relationship

Scheme 6 shows the basic structure of the investigated molecules. Methyl and benzyl were used as substituents R. In both cases, the nitrogen is covalently bonded to an alkyl group. Considering this similarity, the differences found experimentally and computationally are quite large. This suggests that electron

© 2023 The Authors. Chemistry - A European Journal published by Wiley-VCH GmbH

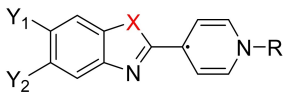

Scheme 6. Schematic representation of 2-(4-R-phenyl)-6-Y-benzo[*d*]-X-zole investigated in this study with X=O, S, NH, NMe; $Y_{1,2}$=H, Me; R=Me, Bn.

donating or withdrawing substituents R (e.g., fluoro alkanes) could have a rather large effect on the redox potential. For the heteroatom X, oxygen and sulfur, give very similar redox potentials that are highly reversible. Switching X to NH or NMe decreases the redox potentials by 0.2 V. However, the redox reactions are no longer reversible. The computational investigations suggest that dimer formation through hydrogen bonds, van der Waals interaction or interaction with chloride ions, may have relevance for these molecules.

Conclusions

A combination of theoretical and experimental studies allows the screening of new active materials for organic batteries. In this work, basic structures such as benzothiazole, -oxazole and -imidazole were synthesized in the most efficient way. Furthermore, they are calculated (at DFT-D3 level of theory) to evidence the principles that serve as the foundation for a theoretical screening study. Their electrochemical properties were investigated in solution by cyclic voltammetry; this provided the first information about the redox potentials and stabilities of the compounds. In general, two reduction/oxidation ($E_{1/2}$ reduction and $E_{1/2}$ oxidation) processes were observed for the investigated compounds, but the first one turned out to be more stable with time and at different scanning speeds. Based on the experimental results in combination with the theoretical ones as a first outcome, it can be said that the most promising class of molecules for further investigations are the benzoxazoles derivates. They give a −1.10 V half-wave potential experimentally and computationally for the first reduction/oxidation. Importantly, they maintain the reversibility of the redox reaction when holding time and different scanning speed were applied. Conversely, benzimidazoles did not exhibit reversible behavior during cyclic voltammetry measurements. Additionally, the computational results indicate that compounds **7** and **9** exhibit ion pair and dimer formation. Both need to be further investigated in detail to give a more comprehensive conclusion regarding the processes occurring with the -imidazole derivatives while reduction/oxidation.

In the end of this part of the research, we can state that benzoxazoles molecules exhibit the better electrochemical properties than benzothiazole and -imidazole molecules and will further be introduced into or onto a polymeric backbone, with the aim of being used in organic polymer batteries.

The overall agreement between the experimental and the computational results indicates the feasibility of using computational high-throughput screening for a wide range of molecules with the same basic structures.

Experimental Section

Synthesis of 2-(pyridine-4-yl)benzoxazole: The synthesis of was adapted from a literature procedure.[32–33]

Equimolar amounts of 2-aminophenol and isonicotinic acid were mixed with polyphosphoric acid (2.5 g for mmol). The mixture was slowly heated under argon to 210 °C (±5 °C) for 3 h. The solution was cooled to about 100 °C, and poured into 100 mL of iced water. It was neutralized with 1 M NaOH while rapidly stirring, the precipitate was filtered, and the crude product was dissolved with a mixture of EtOAc and acetone for purification (8.92 g, 83 %). ^{1}H NMR (300 MHz, [D]chloroform) δ: 7.37–7.51 (m, 2 H, $CH_{benzoxazole}$-$CH_{benzoxazole}$), 7.65 (br d, J=6.85 Hz, 1 H, $CH_{benzoxazole}$-C–N), 7.79–7.90 (m, 1 H, $CH_{benzoxazole}$-C–O), 8.11 (br d, J=5.25 Hz, 2 H, $CH_{pyridine}$), 8.85 ppm (br d, J=5.25 Hz, 2 H, $CH_{pyridine}$-N). ^{13}C NMR (75 MHz, [D]chloroform): δ=110.95 ($CH_{benzoxazole}$-C–O), 120.69 ($CH_{benzoxazole}$-C–N), 120.99 ($CH_{pyridine}$), 125.13 ($CH_{benzoxazole}$), 126.31 ($CH_{benzoxazole}$), 134.33 ($C_{benzoxazole}$-N), 141.76 ($C_{pyridine}$), 150.76 ($CH_{pyridine}$-N), 150.87 ($C_{benzoxazole}$-O), 160.64 ppm ($C_{benzoxazole}$-$C_{pyridine}$). Elemental analysis calcd (%) for $C_{12}H_8N_2O$+0.066 H_2O: C 73.02, H 4.15, N 14.19; found: C 73.04, H 4.03, N 14.19. LC data can be found in the Supporting Information.

Synthesis of 4-(4-methylbenzoxazole)pyridine: 4-(4-Methylbenzoxazole)pyridine was synthesized using the same procedure as 2-(pyridin-4-yl)benzoxazole. Instead of 2-amino-phenol, 2-amino-4-methylphenol (6 g, 48.72 mmol) was used to introduce the pyridine substituent (9.14 g, 90 %). ^{1}H NMR (300 MHz, [D]chloroform): δ=2.52 (s, 3 H, CH_3-$C_{benzoxazole}$), 7.23–7.28 (m, 1 H, $CH_{benzoxazole}$), 7.51 (d, J=8.22 Hz, 1 H, $CH_{benzoxazole}$-C–N), 7.62 (s, 1 H, $CH_{benzoxazole}$-C–O), 8.06–8.12 (m, 2 H, $CH_{pyridine}$), 8.80–8.86 ppm (m, 2 H, $CH_{pyridine}$-N). ^{13}C NMR (75 MHz, [D]chloroform): δ=21.52 (CH_3-$C_{benzoxazole}$), 110.29 ($CH_{bezoxazole}$-C–O), 120.48 ($CH_{benzoxazole}$-C–N), 120.93 ($CH_{pyridine}$) 127.52 ($CH_{benzoxazole}$), 134.49 ($C_{benzoxazole}$-CH_3), 135.07 ($C_{benzoxazole}$-N), 141.97 ($C_{pyridine}$), 149.15 ($C_{pyridine}$-N), 150.71 ($C_{benzoxazole}$-O), 160.68 ppm ($C_{benzoxazole}$-$C_{pyridine}$). Elemental analysis calcd (%) for $C_{13}H_{10}N_2O$: C 74.27, H 4.79, N 13.33; found: C 74.17, H 4.76, N 13.32. LC data can be found in the Supporting Information.

Synthesis of 4-(5-methylbenzoxazole)pyridine: 4-(5-Methylbenzoxazole)pyridine was synthesized using the same procedure as 2-(pyridin-4-yl)benzoxazole. Instead of 2-amino-phenol, 2-amino-5-methylphenol (6 g, 48.72 mmol) was used to introduce the pyridine substituent (9.34 g, 91.24 %). ^{1}H NMR (300 MHz, [D]chloroform): δ=2.55 (s, 3 H, CH_3-$C_{benzoxazole}$), 7.24 (d, J=8.22 Hz, 1 H, $CH_{benzoxazole}$), 7.44 (s, 1 H, $CH_{benzoxazole}$-C–O), 7.70 (d, J=8.22 Hz, 1 H, $CH_{benzoxazole}$-C–N)), 8.04–8.12 (m, 2 H, $CH_{pyridine}$), 8.79–8.86 ppm (m, 2 H, $CH_{pyridine}$-N). ^{13}C NMR (75 MHz, [D]chloroform): δ=21.90 (CH_3-$C_{benzoxazole}$), 111.02 ($CH_{bezoxazole}$-C–O), 119.99 $CH_{benzoxazole}$-C–N), 120.86 ($CH_{pyridine}$), 126.47 ($CH_{benzoxazole}$), 134.50 ($C_{benzoxazole}$-CH_3), 137.00 ($C_{benzoxazole}$-N), 139.62 ($C_{pyridine}$), 150.69 ($C_{pyridine}$-N), 151.18 ($C_{benzoxazole}$-O), 160.11 ppm ($C_{benzoxazole}$-$C_{pyridine}$). Elemental analysis calcd (%) for $C_{13}H_{10}N_2O$+0.066 H_2O: C 73.85, H 4.83, N 13.25; found: C 73.91, H 4.72, N 13.22. LC data can be found in the Supporting Information.

Synthesis of 4-(benzoxazol-2-yl)-1-methylpyridinium chloride: 0.5 g (2.55 mmol) 2-(Pyridin-4-yl)benzoxazole was dissolved in 2.5 mL dichloromethane. 0.376 g (164.99 µL, 2.65 mmol) Methyl iodide was added resultingto a red solution After an initial rise in the reaction mixture's temperature, a precipitate was formed. The suspension was stirred at room temperature for 1 h and afterwards at reflux for additional 1 h. The precipitate was filtered of, washed with dichloromethane (3×5 mL), dried and dissolved in 12.5 mL

© 2023 The Authors. Chemistry - A European Journal published by Wiley-VCH GmbH

deionized water. 1.25 g Dowex Marathon A2 was added and the solution was stirred for 2 h. The ion exchange resin was filtered off, and the solution was freeze dried. The product formed as a yellow solid (0.48 g, 76.35 %). ^{1}H NMR (300 MHz, D_2O): $\delta = 4.38$ (s, 3 H, N^+-CH_3), 7.40–7.47 (m, 1 H, $CH_{benzoxazole}$), 7.47–7.55 (m, 1 H, $CH_{benzoxazole}$), 7.68 (d, $J = 8.22$ Hz, 1 H, $CH_{benzoxazole}$-C–N), 7.75 (d, $J = 7.54$ Hz, 1 H, $CH_{bezoxazole}$-C–O), 8.51 (d, $J = 6.62$ Hz, 2 H, $CH_{pyridine}$), 8.87 ppm (d, $J = 6.62$ Hz, 2 H, $CH_{pyridine}$-N^+). ^{13}C NMR (75 MHz, D_2O): $\delta = 48.31$ (N^+-CH_3), 111.79 ($CH_{bezoxazole}$-C–O), 120.70 ($CH_{bezoxazole}$-C–N), 124.82 ($CH_{pyridine}$), 126.26 ($CH_{benzoxazole}$), 128.54 ($CH_{benzoxazole}$), 140.53 ($C_{benzoxazole}$-N), 140.71 ($C_{pyridine}$), 146.20 ($C_{benzoxazole}$-O), 151.02 ($CH_{pyridine}$-N^+), 157.57 ppm ($C_{benzoxazole}$-$C_{pyridine}$). Elemental analysis calcd (%) for $C_{13}H_{11}N_2OCl + 0.03\ CH_2Cl + 0.8\ H_2O$: C 59.36, H 4.84, N 10.63, Cl 14.25; found: C 59.15, H 4.55, N 10.51, Cl 14.49. LC data can be found in the Supporting Information.

Synthesis of 1-methyl-4-(5-methylbenzo[*d*]oxazol-2-yl)pyridin-1-ium chloride: The title compound was synthesized using the same procedure as 4-(benzoxazol-2-yl)-1-methylpyridinium chloride. Instead of 2-(pyridin-4-yl)benzoxazole, 4-(4-methylbenzoxazole) pyridine (0.7 g, 3.33 mmol) was used (0.2 g, 23 %). ^{1}H NMR (300 MHz, D_2O): $\delta = 2.35$ (s, 3 H, CH_3-$C_{benzoxazole}$), 4.37 (s, 3 H, CH_3-N^+), 7.30 (dd, $J = 8.45$, 1.37 Hz, 1 H, $CH_{benzoxazole}$-C–O), 7.48–7.54 (m, 2 H, $CH_{benzoxazole} + CH_{benzoxazole}$-C–N), 8.46 (d, $J = 7.08$ Hz, 2 H, $CH_{pyridine}$), 8.86 ppm (d, $J = 6.85$ Hz, 2 H, $CH_{pyridine}$-N^+). ^{13}C NMR (75 MHz, D_2O): $\delta = 20.51$ (CH_3-$C_{benzoxazole}$), 48.28 (CH_3-N^+), 111.17 ($CH_{benzoxazole}$-C–O), 120.11 ($CH_{benzoxazole}$-C–N), 124.66 ($CH_{pyridine}$), 129.84 ($CH_{benzoxazole}$), 136.84 ($C_{benzoxazole}$-CH_3), 140.69 ($C_{benzoxazole}$-N), 146.13 ($C_{benzoxazole}$-O + $CH_{pyridine}$-N^+), 149.28 ($C_{pyridine}$), 157.49 ppm ($C_{benzoxazole}$-$C_{pyridine}$). Elemental analysis calcd (%) for $C_{14}H_{13}N_2OCl + 1.05\ H_2O$: C 60.13, H 5.44, N 10.02, Cl 12.68; found: C 60.14, H 5.35, N 10.53, Cl 12.18. LC data can be found in the Supporting Information.

Synthesis of 1-methyl-4-(6-methylbenzo[*d*]oxazol-2-yl)pyridin-1-ium chloride: The title compound was synthesized using the same procedure as 4-(benzooxazol-2-yl)-1-methylpyridinium chloride. Instead of 2-(pyridin-4-yl)benzoxazole, 4-(5-methylbenzoxazole) pyridine (0.5 g, 2.38 mmol) was used (0.08 g, 12.9 %). ^{1}H NMR (300 MHz, D_2O): $\delta = 2.40$ (s, 3 H, CH_3-$C_{benzoxazole}$), 4.37 (s, 3 H, CH_3-N^+), 7.23 (d, $J = 8.22$ Hz, 1 H, $CH_{benzoxazole}$), 7.45 (s, 1 H, $CH_{benzoxazole}$-C–O), 7.55 (d, $J = 8.22$ Hz, 1 H, $CH_{benzoxazole}$-C–N), 8.44 (d, $J = 6.62$ Hz, 2 H, $CH_{pyridine}$), 8.85 ppm (d, $J = 6.62$ Hz, 2 H, $CH_{pyridine}$-N^+). ^{13}C NMR (75 MHz, D_2O): $\delta = 21.08$ (CH_3-$C_{benzoxazole}$), 48.25 (CH_3-N^+), 111.54 ($CH_{benzoxazole}$-C–O), 120.00 ($CH_{benzoxazole}$-C–N), 124.53 ($CH_{pyridine}$), 127.67 ($CH_{benzoxazole}$), 138.37 ($C_{benzoxazole}$-CH_3), 140.14 ($C_{benzoxazole}$-N), 140.66 ($C_{benzoxazole}$-O), 146.09 ($CH_{pyridine}$-N^+), 151.30 ($C_{pyridine}$), 156.90 ppm ($C_{benzoxazole}$-$C_{pyridine}$). Elemental analysis calcd (%) for $C_{14}H_{13}N_2OCl + 1.21\ H_2O$: C 59.52, H 5.5, N 9.92, Cl 12.55; found: C 59.58, H 5.39, N 9.87, Cl 12.85. LC data can be found in the Supporting Information.

Synthesis of 4-(benzooxazol-2-yl)-1-benzylpyridinium chloride: 2-(Pyridin-4-yl)benzoxazole (2.00 g, 10.2 mmol) was dissolved in 25 mL dichloromethane. 1.31 g (1.20 mL, 10.4 mmol) benzyl chloride and catalytical amounts of potassium iodide were added to the resulting red solution. The suspension was stirred at room temperature for 30 min. A slow formation of precipitate was visible. Afterwards the mixture was heated to reflux and stirred for 3 h. After cooling to room temperature, the precipitate was filtered of, washed with dichloromethane (3×20 mL), and dried under reduced pressure. The solid was dissolved in 50 mL deionized water and 1 g Dowex Marathon A2 was added and the solution was stirred for 1 h. The ion exchange resin was filtered off, and the solution was freeze dried. The product formed as orange solid (2.78 g, 87 %). ^{1}H NMR (300 MHz, D_2O): $\delta = 6.03$ (s, 2H, N^+-CH_2), 7.42–7.66 (m, 7H, –C–$CH_{benzoxazole}$, C_{benzyl}), 7.97 (dd, $J = 16.33$, 7.88 Hz, 2H, $CH_{benzoxazole}$-$CH_{benzoxazole}$), 8.79 (d, $J = 6.85$ Hz, 2H, $CH_{pyridine}$), 9.49 ppm (d, $J = 6.85$ Hz, 2H, $CH_{pyridine}$-N^+). ^{13}C NMR (75 MHz, D_2O): $\delta = 63.66$ (N-CH_2), 112.28 ($CH_{benzoxazole}$-C–N), 121.76 ($CH_{benzoxazole}$-C–O), 125.08 ($CH_{pyridine}$), 126.62 + 128.77 ($CH_{benzoxazole}$-$CH_{benzoxazole}$), 129.55 + 129.74 + 129.97 + 134.64 (C_{benzyl}), 141.27 + 141.67 ($C_{benzoxazole}$-N + $C_{benzoxazole}$-O), 146.52 ($CH_{pyridine}$-N^+), 151.34 ($C_{pyridine}$), 158.11 ppm ($C_{benzoxazole}$-$C_{pyridine}$). HRMS (ESI *m/z*): calcd (%) for $[C_{19}H_{15}N_2O]^+$ 287.1179 found 287.1227. Elemental analysis calcd (%) for $C_{13}H_{11}N_2OCl + 0.55\ H_2O$: C 60.85, H 4.75, N 10.92, Cl 13.82; found: C 60.86, H 4.76, N 10.85, Cl 13.86.

Synthesis of 2-(pyridin-4-yl)benzothiazole: 2-Aminobenzenethiol (30 g, 25.6 mL, 240 mmol) and pyridine 4-carbaldehyde (28 g, 24.5 mL, 263 mmol) were dissolved in 500 mL dimethyl sulfoxide. Afterwards, 50 g (263 mmol) sodium metabisulfite was added portionwise. The suspension was heated to 120 °C and turned into an orange solution, which turned black over time. The reaction mixture was stirred at 120 °C for 16 h. After cooling to room temperature, the solution was purred into 4 L deionized water. The resulting precipitate was washed with water (3×150 mL). The desired product was recrystallized from methanol as a colorless solid after (41.8 g, 82 %). ^{1}H NMR (300 MHz, [D]chloroform): $\delta = 7.39$–7.61 (m, 2H, $CH_{benzothiazole}$), 7.89–7.99 (m. 3H, $CH_{benzothiazole}$-C–S, $CH_{pyridine}$), 8.14 (d, $J = 7.54$ Hz, 1H, $CH_{benzothiazole}$-C–N), 8.78 ppm (d, $J = 7.54$ Hz, 2H, $CH_{pyridine}$-N). ^{13}C NMR (75 MHz, [D]chloroform): $\delta = 121.18$ ($CH_{pyridine}$), 121.87 ($CH_{benzothiazole}$-C–N), 123.82 ($CH_{benzothiazole}$-C–S), 127.89 + 126.82 ($CH_{benzothiazole}$), 135.21 ($C_{benzoxazole}$-N), 140.46 ($C_{benzoxazole}$-O), 150.78 ($CH_{pyridine}$-N), 153.97 ($C_{pyridine}$),165.10 ppm ($C_{benzoxazole}$-$C_{pyridine}$). HRMS (ESI *m/z*): calcd (%) for $[C_{12}H_8N_2S + H]^+$ 213.0481 found 213.0502. Elemental analysis calcd (%) for $C_{12}H_8N_2S$: C 67.90, H 3.80, N 13.20, S 15.10; found: C 67.86, H 3.74, N 13.27, S 15.03.

Synthesis of 4-(benzothiazol-2-yl)-1-methylpyridinium chloride: 2-(Pyridin-4-yl)benzothiazole (2.00 g, 9.42 mmol) was dissolved in 12 mL dichloromethane. Methyl iodide (1.47 g, 645 μL, 10.4 mmol) was added to the received red solution. After an initial rise in the reaction mixture's temperature, a precipitate was formed. The suspension was stirred at room temperature for 1 h and afterwards at reflux for additional 3 h. The precipitate was filtered of, washed with dichloromethane (3×20 mL), dried, and dissolved in 50 mL deionized water. Dowex Marathon A2 (5 g) was added, and the solution was stirred for 2 h. The ion-exchange resin was filtered off, and the solution was freeze dried. The product formed as a yellow solid (2.21 g, 95 %). ^{1}H NMR (300 MHz, D_2O): $\delta = 4.25$ (s, 3H, N^+-$CH3$), 7.44–7.58 (m, 2H, C–$CH_{benzothiazole}$), 7.84–7.92 (m, 2H, $CH_{benzothiazole}$-$CH_{benzothiazole}$), 8.15 (d, $J = 6.85$ Hz, 2H, $CH_{pyridine}$), 8.61 ppm (d, $J = 6.62$ Hz, 2H, $CH_{pyridine}$-N^+). ^{13}C NMR (75 MHz, D_2O): $\delta = 48.34$(N-CH_3), 110.94 ($CH_{benzothiazole}$-C–N), 120.67 ($CH_{benzothiazole}$-C–S), 120.99 ($CH_{pyridine}$), 125.13 + 126.31 ($CH_{benzothiazole}$-$CH_{benzothiazole}$), 134.32 + 141.73 ($C_{benzothiazole}$-N + $C_{benzothiazole}$-S), 150.72 ($CH_{pyridine}$-N^+), 150.84 ($C_{pyridine}$), 160.59 ppm ($C_{benzothiazole}$-$C_{pyridine}$). HRMS (ESI *m/z*): calcd (%) for $[C_{13}H_{11}N_2S]^+$ 227.0637 found 227.0617. Elemental analysis calcd (%) for $C_{13}H_{11}N_2SCl + 0.55\ H_2O$: C 56.63, H 4.55, N 10.16, S 11.63, Cl 12.86; found: C 56.72, H 4.46, N 10.23, S 11.52, Cl 12.82.

Synthesis of 4-(benzothiazol-2-yl)-1-benzylpyridinium chloride: 2-(Pyridin-4-yl)benzothiazole (2.00 g, 9.4 mmol) was dissolved in 12 mL dichloromethane. benzyl chloride (1.31 g, 1.20 mL, 10.4 mmol) and catalytical amounts of potassium iodide were added to the resulting red solution. The suspension was stirred at room temperature for 30 min. A slow formation of precipitate was visible. Afterwards the mixture was stirred for additional 24 h. After cooling to room temperature, the precipitate was filtered of, washed with dichloromethane (3×10 mL) and dried under reduced pressure. The solid was dissolved in 50 mL deionized water, and 1 g Dowex Marathon A2 was added and the solution was stirred for 1 h. The ion exchange resin was filtered off, and the solution was freeze dried. The product formed as a yellow solid (2.88 g, 95 %). ^{1}H NMR (300 MHz, [D_6]DMSO): $\delta = 5.97$ (s, 2H, N^+-CH_2), 7.41–7.72 (m, 7H, –C–$CH_{benzothiazole}$, C_{benzyl}), 8.23–8.38 (m, 2H, $CH_{benzothiazole}$-

© 2023 The Authors. Chemistry - A European Journal published by Wiley-VCH GmbH

$CH_{benzothiazole}$), 8.78 (d, $J=6.85$ Hz, 2H, $CH_{pyridine}$), 9.39 ppm (d, $J=7.08$ Hz, 2H, $CH_{pyridine}$-N^+). ^{13}C NMR (75 MHz, [D_6]DMSO): $\delta=63.48$ (N-CH_2), 123.69 ($CH_{benzothiazole}$-C–N), 124.84 ($CH_{benzothiazole}$-C–S), 125.80 ($CH_{pyridine}$), 128.33 + 129.40 + 129.74 + 129.90 (C_{benzyl}), 134.68 + 136.70 ($CH_{benzothiazole}$-$CH_{benzothiazole}$), 146.36 ($CH_{pyridine}$-N^+), 147.14 ($C_{benzothiazole}$-N + $C_{benzothiazole}$-S), 153.83 ($C_{pyridine}$), 161.79 ppm ($C_{benzothiazole}$-$C_{pyridine}$). HRMS (ESI *m/z*): calcd for $[C_{19}H_{15}N_2S]^+$: 303.0950; found 303.0927. Elemental analysis calcd (%) for $C_{19}H_{15}N_2SCl + 0.1\ HCl + 1.3\ H_2O$: C 62.37, H 4.88, N 7.66, S 8.76, Cl 10.66; found: C 62.26, H 4.66, N 7.76, S 8.76, Cl 10.63.

Synthesis of 2-(pyridin-4-yl)-1*H*-benzoimidazole: 1,2-Diaminobenzene (200 g, 185 mmol) and pyridine 4-carbaldehyde (21.6 g, 19.0 mL, 203 mmol) were dissolved in 500 mL dimethyl sulfoxide. Afterwards 38.7 g (203 mmol) sodium metabisulfite was added portionwise. The suspension was heated to 120 °C and turned into an orange solution, which turned black over time. The reaction mixture was stirred at 120 °C for 16 h. After cooling to room temperature, the solution was purred into 4 L deionized water. The resulting precipitate was washed with water (3×150 mL). The desired product was recrystallized from methanol as a colorless solid (25.08 g, 70 %). ^1H NMR (300 MHz, [D_6]DMSO): $\delta=6.34$–6.49 (m, 2H, $CH_{benzoimidazole}$-$CH_{benzoimidazole}$), 6.68–6.92 (m. 2H, $CH_{benzoimidazole}$-C–N), 7.24 (d, $J=4.95$ Hz, 2H, $CH_{pyridine}$), 7.90 (d, $J=4.94$ Hz, 2H, $CH_{pyridine}$-N), 12.41 ppm (br s, 1H, NH). ^{13}C NMR (75 MHz, [D_6]DMSO): $\delta=120.78$ ($CH_{pyridine}$ + $CH_{benzoimidazole}$-C–N), 123.37 ($CH_{benzoimidazole}$-$CH_{benzoimidazole}$), 137.59 ($C_{benzoimidazole}$-N + $C_{pyridine}$), 149.21 ($CH_{pyridine}$-N), 150.95 ppm ($C_{benzoxazole}$-$C_{pyridine}$). HRMS (ESI *m/z*): calcd for $[C_{12}H_9N_3+H]^+$: 196.0869 found 196.0909. Elemental analysis calcd (%) for $C_{12}H_9N_3$: C 73.83, H 4.56, N 21.51; found: C 73.66, H 4.56, N 21.51.

Synthesis of 4-(1*H*-benzoimidazol-2-yl)-1-methylpyridinium chloride: 2-(Pyridin-4-yl)-1*H*-benzoimidazole (4.00 g, 20.5 mmol) was dissolved in 200 mL acetone. Methyl iodide (3.20 g, 140 mL, 22.54 mmol) was added to the resulting red solution. After an initial rise in the reaction mixture's temperature, a precipitate formed. The suspension was stirred at room temperature for 1 h and afterwards at reflux for additional 2 h. The precipitate was filtered of, washed with dichloromethane (3×20 mL), dried and dissolved in 50 mL deionized water. Dowex Marathon A2 (5 g) was added, and the solution was stirred for 2 h. The ion exchange resin was filtered off, and the solution was freeze dried. The product formed as a yellow solid (4.80 g, 95 %). ^1H NMR (300 MHz, D_2O): $\delta=3.84$ (s, 3H, N^+-$CH3$), 6.76–6.85 (m, 2H, C–$CH_{benzoimidazole}$), 6.85–6.94 (m, 2H, $CH_{benzoimidazole}$-$CH_{benzoimidazole}$), 7.08 (d, $J=6.85$ Hz, 2H, $CH_{pyridine}$), 7.92 ppm (d, $J=6.65$ Hz, 2H, $CH_{pyridine}$-N^+). ^{13}C NMR (75 MHz, D_2O): $\delta=47.46$(N-CH_3), 115.57 ($CH_{benzoimidazole}$-C–N), 121.78 ($CH_{benzoimidazole}$-$CH_{benzoimidazole}$), 137.51 ($C_{benzothiazole}$-N), 140.55 ($C_{pyridine}$), 143.09 ($C_{benzothiazole}$-$C_{pyridine}$), 144.46 ppm ($CH_{pyridine}$-N^+). HRMS (ESI *m/z*): calcd for $[C_{13}H_{12}N_3]^+$: 210.1026 found 210.1059. Elemental analysis calcd (%) for $C_{13}H_{12}N_3Cl + 0.65\ H_2O$: C 60.66, H 5.21, N 16.32, Cl 13.77; found: C 60.48, H 5.03, N 16.20, Cl 13.71.

Synthesis of 4-(1*H*-benzoimidazol-2-yl)-1-benzylpyridinium chloride: 2-(Pyridin-4-yl)-1*H*-benzoimidazole (2.0 g 10.2 mmol) and benzyl chloride (1.4 g, 1.30 mL, 11.3 mmol) were dispersed in 200 mL acetone. The suspension became a solution upon heating to reflux. After 2 h stirring at reflux, a catalytical amount of potassium iodide was added, and a yellow precipitate formed. The mixture was stirred for additional 2 h at reflux, cooled to room temperature and filtered. The precipitate was washed with 3×10 mL acetone, dried under reduced pressure and dissolved in 50 mL water. Afterwards 5 g ion-exchange resin was added to the solution, and the mixture was stirred for 2 h. The resin was filtered off, and the solution was freeze dried. The desired product was recived as a yellow solid (2.2 g, 67 %). ^1H NMR (300 MHz, [D_6]DMSO): $\delta=5.89$ (s, 2H, N^+-CH_2), 7.26–7.36 (m, 2H, –C–$CH_{benzoimidazole}$), 7.39–7.52 (m, 3H, CH_{benzyl}), 7.56–7.64 (m, 2H, CH_{benzyl}), 7.66–7.76 (m, 2H, $CH_{benzoimidazole}$-$CH_{benzoimidazole}$), 8.87 (d, $J=7.08$ Hz, 2H, $CH_{pyridine}$), 9.33 ppm (d, $J=6.85$ Hz, 2H, $CH_{pyridine}$-N^+). ^{13}C NMR (75 MHz, [D_6]DMSO): $\delta=63.19$ (N-CH_2), 117.04 ($CH_{benzoimidazole}$-C–N), 124.49 ($CH_{benzoimidazole}$-$CH_{benzoimidazole}$), 124.59 ($CH_{pyridine}$), 129.36 + 129.70 + 129.82 + 134.78 (C_{benzyl}), 140.81 ($C_{benzoimidazole}$-N), 153.83 ($C_{pyridine}$), 145.70 ($CH_{pyridine}$-N^+), 146.51 ppm ($C_{benzoimidazole}$-$C_{pyridine}$). HRMS (ESI *m/z*): calcd for $[C_{19}H_{16}N_3]^+$: 286.1339 found 286.1368.

Synthesis of 1-benzyl-4-(1-methyl-1*H*-benzo[*d*]imidazol-2-yl)pyridin-1-ium chloride: 4-(1*H*-Benzoimidazol-2-yl)-1-benzylpyridinium chloride (500 mg, 1.55 mmol) was mixed with 50 mL water-free acetonitrile under argon. Sodium hydride (44.74 mg, 1.86 mmol) was added to the suspension (***CAUTION!*** hydrogen evolution), and the mixture was stirred for 2 h at room temperature. Afterwards 265 mg (116.1 μL, 1.86 mmol) methyl iodide were added, and the reaction mixture was stirred for additional 16 h. The precipitate was filtered off, and the solution was poured into 200 mL ethyl acetate. After 2 h stirring at room temperature the precipitate was filtered off and washed with 3×15 mL dichloromethane. The desired product was produced after drying under reduced pressure as greenish yellow solid (175 mg, 33.5 %). ^1H NMR (300 MHz, [D_6]DMSO): $\delta=4.08$ (s, 3 H, CH_3-$N_{benzoimidazole}$), 5.91 (CH_2-N^+), 7.32–7.53 (m, 5 H, CH_{benzyl}), 7.55–7.63 (m, 2 H, $CH_{benzoimidazole}$), 7.79 (dd, $J=14.05$, 7.88 Hz, 2 H, $CH_{benzoimidazole}$-C–N), 8.60-8.67 (m, 2 H, $CH_{pyridine}$), 9.23–9.31 ppm (m, 2 H, $CH_{pyridine}$-N^+). ^{13}C NMR (75 MHz, [D_6]DMSO): $\delta=32.77$ (CH_3-$N_{benzoimidazole}$), 63.61 (CH_2-N^+), 112.00 ($CH_{imidazole}$-C–N-CH_3), 120.62 ($CH_{pyridine}$), 124.00 ($CH_{benzoimidazole}$), 125.41 ($CH_{benzoimidazole}$), 127.51 ($CH_{benzoimidazole}$-C–N) 129.39 (CH_{benzyl}) 129.82 (CH_{benzyl}) 130.02 CH_{benzyl}), 134.38 (C–CH_2), 137.85 ($C_{benzoimidazole}$-N-CH_3), 142.82 ($C_{pyridine}$), 145.34 ($C_{benzoimidazole}$-N), 145.52 ($CH_{pyridine}$-N^+), 147.41 ppm ($C_{benzoimidazole}$-$C_{pyridine}$). HRMS (ESI *m/z*): calcd for $[C_{13}H_{12}N_3]^+$: 210.1026 found 210.1059.

Computational calculations: To find the starting structures of the molecules, the CREST program package was used.[34–36] First, a conformational search was performed using iterative meta-dynamics with a genetic structure crossing (iMTD-GC) algorithm. Afterwards, a structure optimization using the extended tight-binding approach GFN2-xTB was performed.[37–39] The solvent acetonitrile was described in these calculations with the implicit solvent model analytical linearized Poisson–Boltzmann (ALPB).[40] Conformers were searched up to 125 kJ mol^{-1} above the lowest energy structure. The most promising conformers from this conformational search, together with manually constructed, conformers were calculated using density functional theory (DFT).

All DFT calculations were performed using the software package TURBOMOLE Version 7.5.1.[41–43] The BP86-D3(BJ)/def2-TZVP[44–53] level of theory was applied. The solvent was simulated with the dielectric continuum solvent model COSMO[54–55] (acetonitrile, relative permittivity $\varepsilon_r=37.5$, refractive index $n_D=1.3442$). The calculations were accelerated by replacing the four-center-two-electron integrals of the Coulomb term with three-center-two-electron integrals by means of the resolution-of-identity (RI) approximation.[53,56,57] The "multiple grid" m4 was employed for the quadrature of exchange-correlation terms.[58]

The structures were verified as energetic minima by calculating the vibrational frequencies. The computations were carried out semi numerically at the same theoretical level as the structure optimizations. For this purpose, the TURBOMOLE script NumForce including the fast contribution of the solvent was used.[59–60]

From these vibrational frequency calculations, the ro-vibrational contributions $G^{ro-vib}_{298.15\ K}$ at 298.15 K were determined. As a final step, the structures were reoptimized using BP86-D3(BJ)/def2-TZVP and the DCOSMO-RS solvent model.[61] Furthermore, the outlying charge

© 2023 The Authors. Chemistry - A European Journal published by Wiley-VCH GmbH

correction was applied.[62] This was done to gain the electronic energy E_{elec} of the molecules. The DCOSMO-RS solvent model was not used to calculate $G^{ro-vib}_{298.15\ K}$ because it led to spurious imaginary frequencies during method evaluation.[31] The concentration was adjusted to 1 mol L^{-1} for all molecules by adding a correction term G^{corr}_{conc}, which changes the molar volume used in the translational entropy:

$$G^{corr}_{conc} = -RT \bullet \ln\left(\frac{V^{new}_m}{V^{old}_m}\right) \quad (1)$$

with the molar gas constant R, the temperature T and the new ($V^{new}_m = 0.001\ m^3 mol^{-1}$) and old ($V^{old}_m = 0.02479\ m^3 mol^{-1}$) volume of 1 mol of substance.

The Gibbs energy G° at a temperature of 298.15 K and a concentration of 1 mol L^{-1} was then calculated from:

$$G^\circ = E_{elec} + G^{ro-vib}_{298.15\ K} + G^{corr}_{conc} \quad (2)$$

The calculations were performed for the oxidized, radical and reduced species (Scheme 2). From these data, the oxidation potential E_{Ox} and reduction potential E_{Red} was calculated as following:

$$E_{Ox} = -\frac{\Delta G_{Ox}}{nF} - E_{Ag/AgNO_3} + E^{ox-corr}_{method} \quad (3)$$

$$E_{Red} = -\frac{\Delta G_{Red}}{nF} - E_{Ag/AgNO_3} + E^{red-corr}_{method} \quad (4)$$

Equations (3) and (4) were used with the potential of the Ag/AgNO$_3$ reference electrode $E_{Ag/AgNO_3} = 4.822$ V,[63,64] the Faraday constant F, and the number of electrons n in the half reaction. Moreover, $E^{ox-corr}_{method}$ and $E^{red-corr}_{method}$ in Equations (3) and (4) are system- and method-specific correction terms for the oxidation and reduction potential, respectively.

We determined[31] $E^{ox-corr}_{method} = -159$ mV and $E^{red-corr}_{method} = +40$ mV for these systems and the described approach using BP86-D3(BJ)/def2-TZVP DCOSMO-RS with outlying charge correction.

$$\Delta G_{Ox} = G^o_{298.15\ K}(\text{radical}) - G^o_{298.15\ K}(e^-) - G^o_{298.15\ K}(\text{cation}) \quad (5)$$

$$\Delta G_{Ox} = G^o_{298.15\ K}(\text{anion}) - G^o_{298.15\ K}(e^-) - G^o_{298.15\ K}(\text{radical}) \quad (6)$$

In Equations (5) and (6), $G^\circ_{298.15\ K}(e^-) = -3.632$ kJ mol^{-1} is the Gibbs energy of a free electron.[64] Furthermore, $G^\circ_{298.15\ K}(\text{cation})$, $G^\circ_{298.15\ K}(\text{radical})$ and $G^\circ_{298.15\ K}(\text{anion})$ are the Gibbs energies for the oxidized, radical and reduced species calculated at 298.15 K and 1 mol L^{-1} as described above.

The coordinates of all optimized structures are available at: https://dx.doi.org/10.22029/jlupub-18094.

Acknowledgements

This work was founded by the German Research Foundation (DFG) within priority program "Polymer-based Batteries" (SPP 2248, project number 441217366). We acknowledge computational resources provided by the HPC Core Facility and the HRZ of the Justus-Liebig-University Giessen. Open Access funding enabled and organized by Projekt DEAL.

Conflict of Interests

The authors declare no conflict of interest.

Data Availability Statement

The data that support the findings of this study are available in the supplementary material of this article.

Keywords: anode materials · cyclic voltammetry · density functional theory calculations · redox moieties

[1] C. Samaras, K. Meisterling, *Environ. Sci. Technol.* **2008**, *42*, 3170–3176.
[2] H. Li, Z. Tang, Z. Liu, C. Zhi, *Joule* **2019**, *3*, 613–619.
[3] C. Han, J. Zhu, C. Zhi, H. Li, *J. Mater. Chem. A.* **2020**, *8*, 15479–15512.
[4] N.-K. C. Nair, N. Garimella, *Energy Build.* **2010**, *42*, 2124–2130.
[5] Z. Xing, S. Wang, A. Yu, Z. Chen, *Nano Energy* **2018**, *50*, 229–244.
[6] H. Nishide, K. Oyaizu, *Science* **2008**, *319*, 737–738.
[7] L. Yang, P. Wang, S. Zhang, Y. Wang, L. Zang, H. Zhu, J. Yin, H. Y. Yang, *J. Mater. Chem. A* **2020**, *8*, 22791–22801.
[8] H. Nishide, *Green Chem.* **2022**, *24*, 4650–4679.
[9] N. Goujon, N. Casado, N. Patil, R. Marcilla, D. Mecerreyes, *Prog. Polym. Sci.* **2021**, *122*, 101449.
[10] J. Heiska, M. Nisula, M. Karppinen, *J. Mater. Chem. A* **2019**, *7*, 18735–18758.
[11] E. Schröter, L. Elbinger, M. Mignon, C. Friebe, J. C. Brendel, M. D. Hager, U. S. Schubert, *J. Power Sources* **2023**, *556*, 232293.
[12] T. Janoschka, S. Morgenstern, H. Hiller, C. Friebe, K. Wolkersdörfer, B. Häupler, M. D. Hager, U. S. Schubert, *Polym. Chem.* **2015**, *6*, 7801–7811.
[13] T. Janoschka, N. Martin, U. Martin, C. Friebe, S. Morgenstern, H. Hiller, M. D. Hager, U. S. Schubert, *Nature* **2015**, *527*, 78–81.
[14] M. Chen, L. Liu, P. Zhang, H. Chen, *RSC Adv.* **2021**, *11*, 24429–24435.
[15] N. Sano, W. Tomita, S. Hara, C.-M. Min, J.-S. Lee, K. Oyaizu, H. Nishide, *ACS Appl. Mater. Interfaces* **2013**, *5*, 1355–1361.
[16] L. Striepe, T. Baumgartner, *Chem. Eur. J.* **2017**, *23*, 16924–16940.
[17] M. Kathiresan, B. Ambrose, N. Angulakshmi, D. Elizabeth Mathew, D. Sujatha, A. Manuel Stephan, *J. Mater. Chem. A* **2021**, *9*, 27215–27233.
[18] P. M. S. Monk, *The Viologens, Physicochemical Properties, Synthesis and Applications of the Salts of 4,4′-Bipyridine*, Wiley, Chichester, **1998**.
[19] J. Luo, B. Hu, C. Debruler, T. L. Liu, *Angew. Chem. Int. Ed.* **2018**, *57*, 231–235.
[20] C. S. Sevov, K. H. Hendriks, M. S. Sanford, *J. Phys. Chem. C* **2017**, *121*, 24376–24380.
[21] K. H. Hendriks, C. S. Sevov, M. E. Cook, M. S. Sanford, *ACS Energy Lett.* **2017**, *2*, 2430–2435.
[22] C. S. Sevov, K. H. Hendriks, M. S. Sanford, *JPC C* **2017**, *121*, 24376–24380.
[23] C. S. Sevov, D. P. Hickey, M. E. Cook, S. G. Robinson, S. Barnett, S. D. Minteer, M. S. Sigman, M. S. Sanford, *J. Am. Chem. Soc.* **2017**, *139*, 2924–2927.
[24] P. Savarino, G. Viscardi, P. Quagliotto, P. Perracino, E. Barni, *J. Heterocycl. Chem.* **1997**, *34*, 1479–1485.
[25] J. Scheers, P. Johansson, P. Szczeciński, W. Wieczorek, M. Armand, P. Jacobsson, *J. Power Sources* **2010**, *195*, 6081–6087.
[26] T. H. M. Jonckers, M.-C. Rouan, G. Haché, W. Schepens, S. Hallenberger, J. Baumeister, J. C. Sasaki, *Bioorg. Med. Chem. Lett.* **2012**, *22*, 4998–5002.
[27] S. Schwan, D. Schröder, H. A. Wegner, J. Janek, D. Mollenhauer, *ChemSusChem* **2020**, *13*, 5480–5488.
[28] S. Er, C. Suh, M. P. Marshak, A. Aspuru-Guzik, *Chem. Sci.* **2015**, *6*, 885–893.
[29] L. Cheng, R. S. Assary, X. Qu, A. Jain, S. P. Ong, N. N. Rajput, K. Persson, L. A. Curtiss, *J. Phys. Chem. Lett.* **2015**, *6*, 283–291.
[30] P. T. Kissinger, W. R. Heineman, *J. Chem. Educ.* **1983**, *60*, 702.
[31] A. J. Achazi, Xh. Fataj, P. Rohland, M. D. Hager, U. S. Schubert, D. Mollenhauer, accepted with minor revisionsto *J. Comput. Chem.* **2023**.

© 2023 The Authors. Chemistry - A European Journal published by Wiley-VCH GmbH

[32] D. W. Hein, R. J. Alheim, J. J. Leavitt, *J. Am. Chem. Soc.* **1957**, *79*, 427–429.
[33] H. B. Hepburn, T. J. Donohoe, *Chem. Eur. J.* **2020**, *26*, 1963–1967.
[34] M. Bursch, A. Hansen, P. Pracht, J. T. Kohn, S. Grimme, *Phys. Chem. Chem. Phys.* **2021**, *23*, 287–299.
[35] P. Pracht, S. Grimme, *Chem. Sci.* **2021**, *12*, 6551–6568.
[36] S. Grimme, *J. Chem. Theory Comput.* **2019**, *15*, 2847–2862.
[37] C. Bannwarth, S. Ehlert, S. Grimme, *J. Chem. Theory Comput.* **2019**, *15*, 1652–1671.
[38] S. Grimme, C. Bannwarth, P. Shushkov, *J. Chem. Theory Comput.* **2017**, *13*, 1989–2009.
[39] P. Pracht, E. Caldeweyher, S. Ehlert, S. Grimme, *ChemRxiv* **2019**, 1–19
[40] S. Ehlert, M. Stahn, S. Spicher, S. Grimme, *J. Chem. Theory Comput.* **2021**, *17*, 4250–4261.
[41] S. G. Balasubramani, G. P. Chen, S. Coriani, M. Diedenhofen, M. S. Frank, Y. J. Franzke, F. Furche, R. Grotjahn, M. E. Harding, C. Hättig, A. Hellweg, B. Helmich-Paris, C. Holzer, U. Huniar, M. Kaupp, A. Marefat Khah, S. Karbalaei Khani, T. Müller, F. Mack, B. D. Nguyen, S. M. Parker, E. Perlt, D. Rappoport, K. Reiter, S. Roy, M. Rückert, G. Schmitz, M. Sierka, E. Tapavicza, D. P. Tew, C. van Wüllen, V. K. Voora, F. Weigend, A. Wodyński, J. M. Yu, *J. Chem. Phys.* **2020**, *152*, 184107.
[42] R. Ahlrichs, M. Bär, M. Häser, H. Horn, C. Kölmel, *Chem. Phys. Lett.* **1989**, *162*, 165–169.
[43] S. G. Balasubramani, G. P. Chen, S. Coriani, M. Diedenhofen, M. S. Frank, Y. J. Franzke, F. Furche, R. Grotjahn, M. E. Harding, C. Hättig, A. Hellweg, B. Helmich-Paris, C. Holzer, U. Huniar, M. Kaupp, A. Marefat Khah, S. Karbalaei Khani, T. Müller, F. Mack, B. D. Nguyen, S. M. Parker, E. Perlt, D. Rappoport, K. Reiter, S. Roy, M. Rückert, G. Schmitz, M. Sierka, E. Tapavicza, D. P. Tew, C. van Wüllen, V. K. Voora, F. Weigend, A. Wodyński, J. M. Yu, *J. Chem. Phys.* **2020**, *152*, 184107.
[44] P. A. M. Dirac, R. H. Fowler, *Proc. R. Soc. Lond. Ser. Contain. Pap. Math. Phys. Character* **1929**, *123*, 714–733.
[45] J. C. Slater, *Phys. Rev.* **1951**, *81*, 385–390.
[46] S. H. Vosko, L. Wilk, M. Nusair, *Can. J. Phys.* **1980**, *58*, 1200–1211.
[47] A. D. Becke, *Phys. Rev. A* **1988**, *38*, 3098–3100.
[48] C. Lee, W. Yang, R. G. Parr, *Phys. Rev. B* **1988**, *37*, 785–789.
[49] A. D. Becke, *J. Chem. Phys.* **1993**, *98*, 5648–5652.
[50] S. Grimme, J. Antony, S. Ehrlich, H. Krieg, *J. Chem. Phys.* **2010**, *132*, 154104.
[51] S. Grimme, S. Ehrlich, L. Goerigk, *J. Comput. Chem.* **2011**, *32*, 1456–1465.
[52] F. Weigend, R. Ahlrichs, *Phys. Chem. Chem. Phys.* **2005**, *7*, 3297–3305.
[53] F. Weigend, *Phys. Chem. Chem. Phys.* **2006**, *8*, 1057–1065.
[54] F. Eckert, A. Klamt, *AIChE J.* **2002**, *48*, 369–385.
[55] A. Klamt, G. Schüürmann, *J Chem Soc Perkin Trans 2* **1993**, *5*.
[56] K. Eichkorn, O. Treutler, H. Öhm, M. Häser, R. Ahlrichs, *Chem. Phys. Lett.* **1995**, *240*, 283–290.
[57] K. Eichkorn, O. Treutler, H. Öhm, M. Häser, R. Ahlrichs, *Chem. Phys. Lett.* **1995**, *242*, 652–660.
[58] K. Eichkorn, F. Weigend, O. Treutler, R. Ahlrichs, *Theor. Chem. Acc.* **1997**, *97*, 119–124.
[59] P. Deglmann, F. Furche, *J. Chem. Phys.* **2002**, *117*, 9535–9538.
[60] P. Deglmann, F. Furche, R. Ahlrichs, *Chem. Phys. Lett.* **2002**, *362*, 511–518.
[61] S. Sinnecker, A. Rajendran, A. Klamt, M. Diedenhofen, F. Neese, *J. Phys. Chem. A* **2006**, *110*, 2235–2245.
[62] A. Klamt, V. Jonas, *J. Chem. Phys.* **1996**, *105*, 9972–9981.
[63] V. V. Pavlishchuk, A. W. Addison, *Inorg. Chim. Acta* **2000**, *298*, 97–102.
[64] J. Ho, M. L. Coote, C. J. Cramer, D. G. Truhlar in *Organic Electrochemistry* (Eds.: Ole Hammerich, Bernd Speiser), CRC Press, Boca Raton, **2016**, pp. 229–259.

Manuscript received: September 13, 2023
Accepted manuscript online: November 11, 2023
Version of record online: December 8, 2023

© 2023 The Authors. Chemistry - A European Journal published by Wiley-VCH GmbH